



# CHORUS

This is the accepted manuscript made available via CHORUS. The article has been published as:

## Testing the chiral magnetic effect with isobaric collisions

Wei-Tian Deng, Xu-Guang Huang, Guo-Liang Ma, and Gang Wang

Phys. Rev. C **94**, 041901 — Published 28 October 2016

DOI: [10.1103/PhysRevC.94.041901](https://doi.org/10.1103/PhysRevC.94.041901)

# Testing the chiral magnetic effect with isobaric collisions

Wei-Tian Deng,<sup>1</sup> Xu-Guang Huang,<sup>2,3</sup> Guo-Liang Ma,<sup>4</sup> and Gang Wang<sup>5</sup>

<sup>1</sup>*School of physics, Huazhong University of Science and Technology, Wuhan 430074, China*

<sup>2</sup>*Physics Department and Center for Particle Physics and Field Theory, Fudan University, Shanghai 200433, China*

<sup>3</sup>*Department of Physics, Brookhaven National Laboratory, Upton, New York 11973-5000, USA*

<sup>4</sup>*Shanghai Institute of Applied Physics, Chinese Academy of Sciences, Shanghai 201800, China*

<sup>5</sup>*Department of Physics and Astronomy, University of California, Los Angeles, California 90095, USA*

The quark-gluon matter produced in relativistic heavy-ion collisions may contain local domains in which  $\mathcal{P}$  and  $\mathcal{CP}$  symmetries are not preserved. When coupled with an external magnetic field, such  $\mathcal{P}$ - and  $\mathcal{CP}$ -odd domains will generate electric currents along the magnetic field — a phenomenon called the chiral magnetic effect (CME). Recently, the STAR Collaboration at RHIC and the ALICE Collaboration at the LHC released data of charge-dependent azimuthal-angle correlators with features consistent with the CME expectation. However, the experimental observable is contaminated with significant background contributions from elliptic-flow-driven effects, which makes the interpretation of the data ambiguous. In this Letter, we show that the collisions of isobaric nuclei,  $^{96}_{44}\text{Ru} + ^{96}_{44}\text{Ru}$  and  $^{96}_{40}\text{Zr} + ^{96}_{40}\text{Zr}$ , provide an ideal tool to disentangle the CME signal from the background effects. Our simulation demonstrates that the two collision types at  $\sqrt{s_{\text{NN}}} = 200$  GeV have more than 10% difference in the CME signal and less than 2% difference in the elliptic-flow-driven backgrounds for the centrality range of 20 – 60%.

PACS numbers: 25.75.-q, 12.38.Mh, 25.75.Ag

Quantum chromodynamics (QCD), the modern theory of the strong interaction, permits the violation of parity symmetry ( $\mathcal{P}$ ) or combined charge conjugation and parity symmetry ( $\mathcal{CP}$ ), although accurate experiments performed so far have not seen such violation at vanishing temperature and density [1]. Recently it was suggested that in the hot and dense matter created in high-energy heavy-ion collisions, there may exist metastable domains where  $\mathcal{P}$  and  $\mathcal{CP}$  are violated owing to vacuum transitions induced by topologically nontrivial gluon fields, e.g., sphalerons [2]. In such a domain, net quark chirality can emerge from chiral anomaly, and the strong magnetic field of a non-central collision can then induce an electric current along the magnetic field, which is known as the chiral magnetic effect (CME) [3, 4]; see Refs. [5, 6] for recent reviews of the magnetic field and the CME in heavy-ion collisions.

The CME provides a means to monitoring the topological sector of QCD, and the experimental search for the CME has been intensively performed in heavy-ion collisions at RHIC and the LHC. To detect the CME, a three-point correlator,

$$\gamma_{\alpha\beta} = \langle \cos(\phi_{\alpha} + \phi_{\beta} - 2\Psi_{\text{RP}}) \rangle, \quad (1)$$

was proposed [7], where  $\phi$  is the azimuthal angle of a charged particle, the subscript  $\alpha$  ( $\beta$ ) denotes the charge sign of the particle (positive or negative),  $\Psi_{\text{RP}}$  is the angle of the reaction plane of a given event, and  $\langle \cdot \cdot \cdot \rangle$  denotes an average over all particle pairs and all the events. The occurrence of the CME driven by the magnetic field (perpendicular to the reaction plane) is expected to contribute a positive opposite-sign (OS) correlator and a negative same-sign (SS) correlator. The measurements of the correlator  $\gamma$  by the STAR Collaboration for Au + Au collisions at  $\sqrt{s_{\text{NN}}} = 200$  GeV [8, 9] and by the ALICE Collaboration for Pb + Pb collisions at  $\sqrt{s_{\text{NN}}} = 2.76$  TeV [10], indeed demonstrate the expected features of the CME. The signal is robust against various ways of determination of the reaction plane, and persists when the collision

system changes to Cu + Cu or U + U, and when the collision energy is lowered down to  $\sqrt{s_{\text{NN}}} = 19.6$  GeV [9, 11–13]. For further lowered collision energies, the difference between  $\gamma_{\text{OS}}$  and  $\gamma_{\text{SS}}$  steeply falls down [13], which may be understood by noticing that at lower energies the system is probably in a hadronic phase where the chiral symmetry is broken and the CME is strongly suppressed.

Ambiguities, however, exist in the interpretation of the experimental results, owing to possible background effects that are not related to the CME, e.g., local charge conservation [14–16], transverse momentum conservation [14, 17, 18], etc. These background effects, once coupled with elliptic flow ( $v_2$ ) [19], will contribute to  $\gamma_{\alpha\beta}$ . To disentangle the possible CME signal and the flow-related backgrounds, one can utilize experimental setups to either vary the backgrounds with the signal fixed, or vary the signal with the backgrounds fixed.

The former approach was carried out by exploiting the prolate shape of the uranium nuclei [20]. In central U + U collisions, one expects sizable  $v_2$  but a negligible magnetic field, and thus a vanishingly small CME contribution to the correlator  $\gamma$ . The STAR Collaboration collected 0 – 1% most central events from U + U collisions at  $\sqrt{s_{\text{NN}}} = 197$  GeV in 2012, and indeed found sizable  $v_2$  while the difference between  $\gamma_{\text{OS}}$  and  $\gamma_{\text{SS}}$  (note that the charge-blind backgrounds are subtracted in  $\Delta\gamma$ ),

$$\Delta\gamma \equiv \gamma_{\text{OS}} - \gamma_{\text{SS}}, \quad (2)$$

is consistent with zero [12]. However, it was found that the total multiplicity of detected hadrons is far less dependent on the number of binary collisions than expected [21], so it is very hard to isolate tip-tip collisions (that generate small  $v_2$ ) from body-body collisions (that generate large  $v_2$ ); see also discussions in Ref. [22]. This significantly reduces the lever arm available to manipulate  $v_2$  in order to separate  $v_2$ -driven backgrounds from the CME.

The latter approach (with the  $v_2$ -driven backgrounds fixed)

can be realized, especially for mid-central/mid-peripheral events, with collisions of isobaric nuclei, such as  $^{96}_{44}\text{Ru}$  and  $^{96}_{40}\text{Zr}$  [20]. Ru + Ru and Zr + Zr collisions at the same beam energy are almost identical in terms of particle production, which is illustrated with the Monte Carlo Glauber simulation [23–26] in Fig. 1. The ratio of the multiplicity distributions from the two collision systems is consistent with unity almost everywhere, except in 0 – 5% most central collisions, where the slightly larger radius of Ru ( $R_0 = 5.085$  fm) plays a role against the smaller radius of Zr ( $R_0 = 5.02$  fm). Our centrality bins are defined with the same multiplicity cuts for the two collision types. For the CME analysis, we focus on the centrality range of 20 – 60%, so that the background contributions due to the multiplicity is negligible.

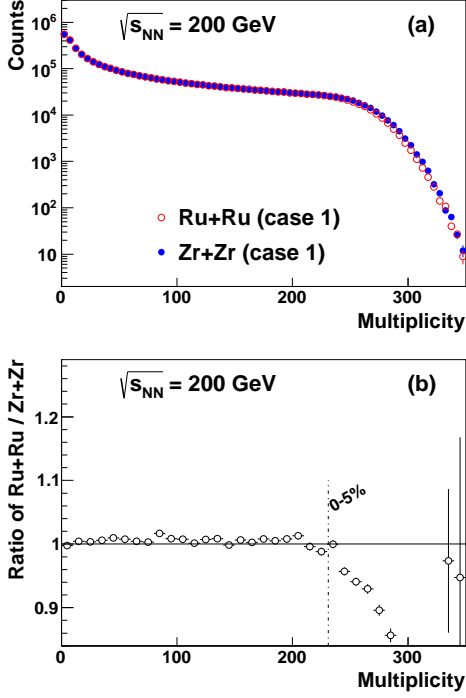


FIG. 1: The Monte Carlo Glauber simulation of the multiplicity distributions for  $^{96}_{44}\text{Ru} + ^{96}_{44}\text{Ru}$  and  $^{96}_{40}\text{Zr} + ^{96}_{40}\text{Zr}$  at  $\sqrt{s_{\text{NN}}} = 200$  GeV (a) and their ratio (b).

The spatial distribution of nucleons in either  $^{96}_{44}\text{Ru}$  or  $^{96}_{40}\text{Zr}$  in the rest frame can be written in the Woods-Saxon form (in spherical coordinates),

$$\rho(r, \theta) = \frac{\rho_0}{1 + \exp[(r - R_0 - \beta_2 R_0 Y_2^0(\theta))/a]}, \quad (3)$$

where  $\rho_0 = 0.16 \text{ fm}^{-3}$  is the normal nuclear density,  $R_0$  and  $a$  represent the “radius” of the nucleus and the surface diffuseness parameter, respectively, and  $\beta_2$  is the deformity of the nucleus. The parameter  $a$  is almost identical for Ru and Zr:  $a \approx 0.46$  fm. Our current knowledge of  $\beta_2$  of Ru and Zr is incomplete. There are two sources of available information on  $\beta_2$  [27]: e-A scattering experiments [28, 29] and comprehensive model deductions [30]. According to the first

source (which will be referred to as case 1), Ru is more deformed ( $\beta_2^{\text{Ru}} = 0.158$ ) than Zr ( $\beta_2^{\text{Zr}} = 0.08$ ); while the second source (which will be referred to as case 2) tells the opposite,  $\beta_2^{\text{Ru}} = 0.053$  is smaller than  $\beta_2^{\text{Zr}} = 0.217$ . As we have checked, this systematic uncertainty has little influence on the multiplicity distribution. We will discuss later its noticeable impacts on the CME signal (via the magnetic field) and the  $v_2$ -driven backgrounds (via  $\epsilon_2$ , the initial spatial eccentricity of the participant zone).

The charge difference between Ru and Zr nuclei provides a handle on the initial magnetic field (mostly produced by the spectator protons) [31, 32]. Figure 2(a) presents the theoretical calculation of the event-averaged initial magnetic field squared with correction from the event-by-event azimuthal fluctuation of the magnetic field orientation,  $B_{sq} \equiv \langle (eB/m_\pi^2)^2 \cos[2(\Psi_B - \Psi_{\text{RP}})] \rangle$  (with  $m_\pi$  the pion mass and  $\Psi_B$  the azimuthal angle of the magnetic field), for the two collision systems at 200 GeV, using the HIJING model [32, 33]. The magnetic field is calculated at the center of mass of the overlapping region.  $B_{sq}$  quantifies the magnetic field’s capability of driving the CME signal in the correlator  $\gamma$  [34, 35]. For the same centrality bin, the Ru + Ru collision produces a significantly stronger magnetic field than Zr + Zr. Some theoretical uncertainties come from the modeling of the nuclei, e.g., how to model the electric charge distribution of the proton: treating the proton as a point charge or as a uniformly charged ball. For the event averaged calculation, this type of uncertainty is small. Another uncertainty involves the Lienard-Wiechert potential used in this calculation, which applied no quantum corrections. At RHIC energies, including corrections from quantum electrodynamics makes little difference [5]. The theoretical uncertainties are greatly suppressed when we take the ratio or relative difference between the two systems. Panel (b) of Fig. 2 shows that the relative difference in  $B_{sq}$  between Ru + Ru and Zr + Zr collisions is approaching 15% (case 1) or 18% (case 2) for peripheral events, and reduces to about 13% (case 1 and case 2) for central events<sup>1</sup>. The effect of the deformity of the nucleus on the generation of the magnetic field is more distinctive in more peripheral collisions.

In Fig. 2(b), we also show the relative difference in the initial eccentricity,  $R_{\epsilon_2}$ , obtained from the Monte Carlo Glauber simulation.  $R_{\epsilon_2}$  is highly consistent with 0 for peripheral events, and goes above (below) 0 for the parameter set of case 1 (case 2) in central collisions, because the Ru (Zr) nucleus is more deformed. The relative difference in  $v_2$  should closely follow that in eccentricity, so for the centrality range of interest, 20 – 60%, the  $v_2$ -related backgrounds should stay almost the same for Ru + Ru and Zr + Zr collisions. The slightly non-zero effect will be taken into account in the significance estimation for the CME signal projection, to be discussed later.

Given the initial magnetic fields and eccentricities, we can

<sup>1</sup> In our notation, the relative difference in a quantity  $F$  between Ru + Ru and Zr + Zr collisions is  $R_F \equiv 2(F^{\text{Ru+Ru}} - F^{\text{Zr+Zr}})/(F^{\text{Ru+Ru}} + F^{\text{Zr+Zr}})$ , and  $F$  can be  $B_{sq}$ ,  $\epsilon_2$  or  $S$ .

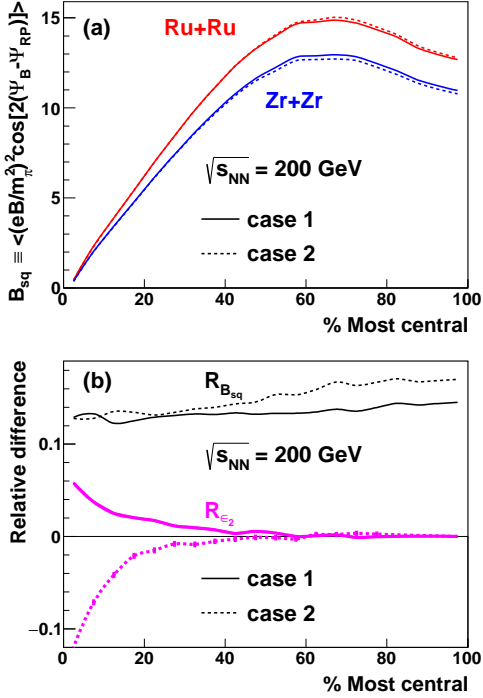


FIG. 2: The event-averaged initial magnetic field squared at the center of mass of the overlapping region with correction from event-by-event fluctuation of its azimuthal orientation for Ru + Ru and Zr + Zr collisions at  $\sqrt{s_{NN}} = 200$  GeV (a) and their relative difference (b) versus centrality. Also shown is the relative difference in initial eccentricity (b). The solid (dashed) lines correspond to the parameter set of case 1 (case 2).

estimate the relative difference in the charge-separation observable  $S \equiv N_{\text{part}} \Delta\gamma$  between Ru + Ru and Zr + Zr collisions. Here  $N_{\text{part}}$  is used to compensate for the dilution effect, which is expected when there are multiple sources involved in the collision [9, 36]. The focus of the isobaric collisions is on the lift of degeneracy between Ru + Ru and Zr + Zr, therefore we express the corresponding  $S$  with a two-component perturbative approach to emphasize the relative difference

$$S^{\text{Ru+Ru}} = \bar{S} \left[ (1 - bg) \left( 1 + \frac{R_{B_{sq}}}{2} \right) + bg \left( 1 + \frac{R_{\epsilon_2}}{2} \right) \right], \quad (4)$$

$$S^{\text{Zr+Zr}} = \bar{S} \left[ (1 - bg) \left( 1 - \frac{R_{B_{sq}}}{2} \right) + bg \left( 1 - \frac{R_{\epsilon_2}}{2} \right) \right], \quad (5)$$

where  $bg \in [0, 1]$  quantifies the background contribution due to elliptic flow and  $\bar{S} = (S^{\text{Ru+Ru}} + S^{\text{Zr+Zr}})/2$ . An advantage of the perturbative approach is that the relative difference in  $S$ ,

$$R_S = (1 - bg)R_{B_{sq}} + bg \cdot R_{\epsilon_2}, \quad (6)$$

is independent of the detailed implementation of  $\bar{S}$ . Without loss of generality, we parametrize  $\bar{S}$  based on the STAR measurements of  $S^{\text{Au+Au}}$  at 200 GeV [11] as a function of

$B_{sq}^{\text{Au+Au}}$ :  $\bar{S} = (2.17 + 2.67\bar{B}_{sq} - 0.074\bar{B}_{sq}^2) \times 10^{-3}$ , where  $\bar{B}_{sq} = (B_{sq}^{\text{Ru+Ru}} + B_{sq}^{\text{Zr+Zr}})/2$ . It is noteworthy that the data points of  $(S, B_{sq})$  for 30 – 60% Cu+Cu collisions at 200 GeV [9] also fall onto this curve. Note that  $\bar{S}$  is almost a linear function of  $\bar{B}_{sq}$  at small  $\bar{B}_{sq}$  values, because the coefficient of the quadratic term is very small.

In Fig. 3(a) we show the projection of  $S^{\text{Ru+Ru}}$  and  $S^{\text{Zr+Zr}}$  at 200 GeV, as functions of centrality, with  $B_{sq}$  and  $\epsilon_2$  obtained for case 1, and the background level  $bg = 2/3$ . The statistical errors are estimated based on 400 million events for each collision type. The gray bands depict the STAR measurements of  $S^{\text{Au+Au}}$  and  $S^{\text{Cu+Cu}}$  at 200 GeV in comparison. For 30 – 60% collisions, all the collision types share a universal curve of  $S(B_{sq})$  or  $\bar{S}(\bar{B}_{sq})$ , which transforms into a rough atomic-number ordering in  $S$  as a function of centrality.

The systematic uncertainties in the projection are largely canceled out with the relative difference between Ru + Ru and Zr + Zr, shown in Fig. 3(b); in comparison, we show again the relative difference in eccentricity. For both parameter sets of the Glauber inputs (red stars for case 1 and pink shaded boxes for case 2), the relative difference in  $S$  is about 5% for centrality range of 20 – 60%. The amounts of  $R_S$  can be easily guessed from the values of  $R_{B_{sq}}$  in Fig. 2(b) scaled down by a factor of 3 (since  $bg = 2/3$  and  $R_{\epsilon_2}$  is close to 0). When we combine the events of 20 – 60% centralities,  $R_S$  is  $5\sigma$  above  $R_{\epsilon_2}$  for both parameter sets of the Glauber inputs. Therefore, the isobaric collisions provide a unique test to pin down the underlying physics mechanism for the observed charge separation. As a by-product,  $v_2$  measurements in central collisions will discern which information source (case 1 or 2) is more reliable regarding the deformity of the Ru and Zr nuclei.

When a different background level is assumed, the magnitude and significance of the projected relative difference between Ru + Ru and Zr + Zr change accordingly, as shown in Fig. 4. The measurements of the isobaric collision data will determine whether there is a finite CME signal observed in the correlator  $\gamma$ , and if the answer is “yes”, will ascertain the background contribution, when compared with this figure. With 400 million events for each collision type, the background level can be determined with an accuracy of 7%.

In summary, we have numerically simulated the strengths of the initial magnetic fields and the participant eccentricities for the isobaric collisions of  $^{96}_{44}\text{Ru} + ^{96}_{44}\text{Ru}$  and  $^{96}_{40}\text{Zr} + ^{96}_{40}\text{Zr}$ . Using the previous STAR measurements of the three-point correlator (1) in Au + Au and Cu + Cu collisions as baseline, we estimate the relative difference in the charge-separation observable  $S = N_{\text{part}} \Delta\gamma$  between Ru + Ru and Zr + Zr collisions, assuming a background level of two thirds. We find a noticeable relative difference in  $S$  which is robust in the 20 – 60% centrality bins. Our results strongly suggest that the isobaric collisions can serve as an ideal tool to disentangle the signal of the chiral magnetic effect from the  $v_2$ -driven backgrounds.

Finally, we point out that the isobaric collisions may also be used to disentangle the signal of the chiral magnetic wave (CMW) [38, 39] from background effects. We summarise in Table I the expected relationship between Ru + Ru and Zr + Zr in terms of experimental observables for elliptic flow, the CME, the CMW and the chiral vortical effect (CVE) [40–

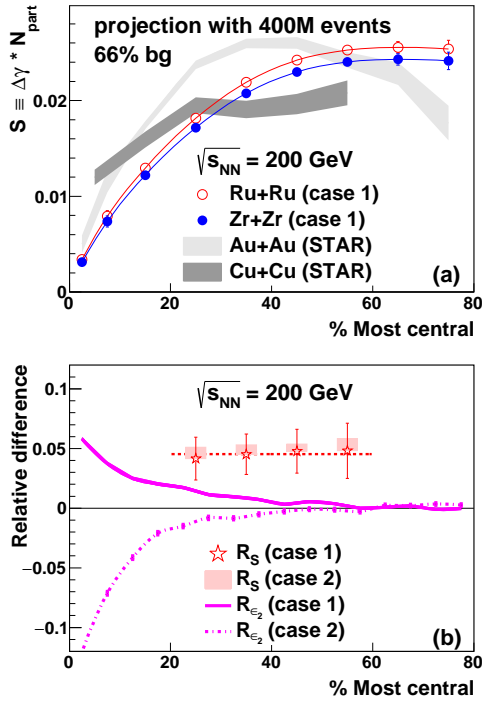


FIG. 3: Projection of  $S \equiv N_{\text{part}}\Delta\gamma$  for Ru + Ru and Zr + Zr collisions at  $\sqrt{s_{\text{NN}}} = 200$  GeV for the parameter set of case 1 (a) and the relative difference in the two (b) versus centrality, assuming the background level to be two thirds. Also shown in panel (b) is the relative difference in the initial eccentricity from the Monte Carlo Glauber simulation (pink solid and dashed lines).

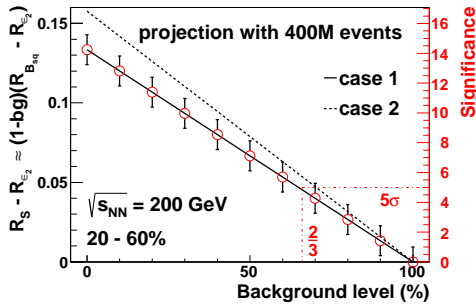


FIG. 4: Magnitude (left axis) and significance (right axis) of the relative difference in the CME signal between Ru + Ru and Zr + Zr at 200 GeV,  $R_S - R_{e_2}$  as a function of the background level.

42], assuming that the chiral effects are the major physical mechanisms for the corresponding observables.

**Acknowledgments:** We are grateful to H. Huang, D. Kharzeev, J. Liao, S. Voloshin, N. Xu, and Z. Xu for helpful communications and discussions. W.-T.D is supported by NSFC with Grant No. 11405066. X.-G.H. is supported by NSFC with Grant No. 11535012 and the One Thousand Young Talents Program of China. G.-L.M is supported by supported by NSFC with Grants No. 11375251, No. 11522547,

TABLE I: The expected relationship between Ru + Ru and Zr + Zr in terms of experimental observables for elliptic flow, the CME, the CMW and the CVE.

Observable	${}^{96}_{44}\text{Ru} + {}^{96}_{44}\text{Ru}$ vs. ${}^{96}_{40}\text{Zr} + {}^{96}_{40}\text{Zr}$
flow	$\approx$
CME	$>$
CMW	$>$
CVE	$\approx$

[1] C. A. Baker *et al.*, Phys. Rev. Lett. **97**, 131801 (2006).  
[2] D. Kharzeev, R. D. Pisarski and M. H. G. Tytgat, Phys. Rev. Lett. **81**, 512 (1998).  
[3] D. E. Kharzeev, L. D. McLerran and H. J. Warringa, Nucl. Phys. A **803**, 227 (2008).  
[4] K. Fukushima, D. E. Kharzeev and H. J. Warringa, Phys. Rev. D **78**, 074033 (2008).  
[5] X. G. Huang, Rept. Prog. Phys. **79**, 076302 (2016).

No. 11421505, and the Major State Basic Research Development Program in China with Grant No. 2014CB845404. G.W is supported by the US Department of Energy under Grants No. DE-FG02-88ER40424.

[6] D. E. Kharzeev, J. Liao, S. A. Voloshin and G. Wang, Prog. Part. Nucl. Phys. **88**, 1 (2016).  
[7] S. A. Voloshin, Phys. Rev. C **70**, 057901 (2004).  
[8] B. I. Abelev *et al.* [STAR Collaboration], Phys. Rev. Lett. **103**, 251601 (2009).  
[9] B. I. Abelev *et al.* [STAR Collaboration], Phys. Rev. C **81**, 054908 (2010).  
[10] B. Abelev *et al.* [ALICE Collaboration], Phys. Rev. Lett. **110**,

- 012301 (2013).
- [11] L. Adamczyk *et al.* [STAR Collaboration], Phys. Rev. C **88**, 064911 (2013).
- [12] G. Wang [STAR Collaboration], Nucl. Phys. A **904-905**, 248c (2013).
- [13] L. Adamczyk *et al.* [STAR Collaboration], Phys. Rev. Lett. **113**, 052302 (2014).
- [14] S. Pratt, arXiv:1002.1758 [nucl-th].
- [15] S. Schlichting and S. Pratt, arXiv:1005.5341 [nucl-th].
- [16] S. Schlichting and S. Pratt, Phys. Rev. C **83**, 014913 (2011).
- [17] S. Pratt, S. Schlichting and S. Gavin, Phys. Rev. C **84**, 024909 (2011).
- [18] A. Bzdak, V. Koch and J. Liao, Phys. Rev. C **83**, 014905 (2011).
- [19] A. M. Poskanzer and S. Voloshin, Phys. Rev. C **58**, 1671 (1998).
- [20] S. A. Voloshin, Phys. Rev. Lett. **105**, 172301 (2010).
- [21] L. Adamczyk *et al.* [STAR Collaboration], Phys. Rev. Lett. **115**, 222301 (2015).
- [22] S. Chatterjee and P. Tribedy, Phys. Rev. C **92**, 011902 (2015).
- [23] K. Adcox *et al.* [PHENIX Collaboration], Phys. Rev. Lett. **86**, 3500 (2001).
- [24] I. G. Bearden *et al.* [BRAHMS Collaboration], Phys. Lett. B **523**, 227 (2001).
- [25] B. B. Back *et al.* [PHOBOS Collaboration], Phys. Rev. C **65**, 061901 (2002).
- [26] [STAR Collaboration], nucl-ex/0311017.
- [27] Q. Y. Shou, Y. G. Ma, P. Sorensen, A. H. Tang, F. Videbaek and H. Wang, Phys. Lett. B **749**, 215 (2015).
- [28] S. Raman, C. W. G. Nestor, Jr and P. Tikkanen, Atom. Data Nucl. Data Tabl. **78**, 1 (2001).
- [29] B. Pritychenko, M. Birch, B. Singh and M. Horoi, Atom. Data Nucl. Data Tabl. **107**, 1 (2016).
- [30] P. Moller, J. R. Nix, W. D. Myers and W. J. Swiatecki, Atom. Data Nucl. Data Tabl. **59**, 185 (1995).
- [31] V. Skokov, A. Y. Illarionov and V. Toneev, Int. J. Mod. Phys. A **24**, 5925 (2009).
- [32] W. T. Deng and X. G. Huang, Phys. Rev. C **85**, 044907 (2012).
- [33] W. T. Deng and X. G. Huang, Phys. Lett. B **742**, 296 (2015).
- [34] J. Błoczyński, X. G. Huang, X. Zhang and J. Liao, Phys. Lett. B **718**, 1529 (2013).
- [35] J. Błoczyński, X. G. Huang, X. Zhang and J. Liao, Nucl. Phys. A **939**, 85 (2015).
- [36] G. L. Ma and B. Zhang, Phys. Lett. B **700**, 39 (2011).
- [37] A. Bzdak, V. Koch and J. Liao, Lect. Notes Phys. **871**, 503 (2013).
- [38] D. E. Kharzeev and H. U. Yee, Phys. Rev. D **83**, 085007 (2011).
- [39] Y. Burnier, D. E. Kharzeev, J. Liao and H. U. Yee, Phys. Rev. Lett. **107**, 052303 (2011).
- [40] J. Erdmenger, M. Haack, M. Kaminski and A. Yarom, JHEP **0901**, 055 (2009).
- [41] N. Banerjee, J. Bhattacharya, S. Bhattacharyya, S. Dutta, R. Loganayagam and P. Surowka, JHEP **1101**, 094 (2011).
- [42] D. T. Son and P. Surowka, Phys. Rev. Lett. **103**, 191601 (2009).